Received: 14 March 2024 | Revised: 25 September 2024 | Accepted: 6 October 2024

IET Generation, Transmission & Distribution

DOI: 10.1049/gtd2.13298

The Institution of Engineering and Technology | WILEY

ORIGINAL RESEARCH

Towards HVDC interoperability—Vendor agnostic control architecture and quantifying domain of operating point

Dong Chen[1] | Pimonpan Phurappa[2,3,4] | Benjamin Marshall[1] | Adam Scott[1] | Callum Henderson[1]

[1]The National HVDC Centre, SSEN Transmission, Cumbernauld, UK

[2]School of Engineering, University of Edinburgh, Edinburgh, UK

[3]Department of Engineering, University of Exeter, Exeter, UK

[4]Faculty of Engineering, University of Strathclyde, Glasgow, UK

Correspondence
Dong Chen, The National HVDC Centre, SSEN Transmission, Cumbernauld, UK.
Email: dong.chen@sse.com

Funding information
Scottish and Southern Electricity Network Transmission; EPSRC, Grant/Award Number: EP/Y035119/1

Abstract

A vendor agnostic design framework is proposed for multi-terminal high voltage direct current (HVDC) here. An analytical assessment is then proposed as a first step of this assessment to quantify the domain of operating point. The criterion is indexed by the margin against loss-of-equilibrium for an Multi-Vendor-Multi-Terminal (MVMT)-HVDC network with terminal behaviour of connected converters. Based on a multi-terminal control architecture, a static analytical model is established, including relevant parameters within the direct current network, its topology, and operation. Two types of scalar index are proposed and then normalized to indicate the margin against loss-of-equilibrium and then employed to quantify the domain of operating point. It is proposed that the domain of security shall correspond to a value in closer proximity to '1' for better security. The effectiveness of the indices is verified and analysed with simulations in the environments of both Matlab/Simulink and real-time digital simulator with pseudo-steady-state and detailed electro-magnetic transient modelling, respectively. This approach attempts to represent one MVMT control scheme to support practical specification, testing and demonstration of the first MVMT-HVDC control system as a business case.

1 | INTRODUCTION

Mass utilization of offshore wind energy has been identified as an enabler towards a net-zero electricity system by the UK government [1]. Within the holistic network design [2] for the GB system to 2030, a range of multi-terminal high voltage direct current (MT-HVDC) transmission systems have been considered as an effective and economical approach to transmit bulk offshore power to the existing onshore power network [3]. These more extensive direct current (DC) networks which are set to emerge are doing so coincident with an unprecedented growth of demand for HVDC worldwide and the need for transmission system operators (TSOs) to describe staged growth of and control paradigms for these DC networks. In this context, the need for Multi-Vendor-Multi-Terminal (MVMT)-HVDC solutions becomes increasingly likely.

Within Great Braintan (GB), the Caithness–Moray–Shetland project (C–M–S) [4] is the first example of a multi-terminal voltage source converter (VSC)–HVDC system outside of China, although this has been delivered by a single vendor. In pilot projects elsewhere involving multiple vendors, it is understood that the vendors have been required to both open up areas of intellectual property (IP) relating to control design and to modify their designs to make them compatible with other converters. This sort of open IP approach is not practical within GB and other international markets. There is a need for a practical approach to MVMT-HVDC control without the requirement for vendors to divulge IP or for a third party to take responsibility for control design on every converter. The National HVDC Centre and SSEN Transmission are taking forward 'Project Aquila' to demonstrate MVMT-HVDC arrangement, applying control principles that provide for effective interoperability while protecting each vendor's IP.

The principal challenge of MVMT control interoperability is how to ensure HVDC converters of different vendor solutions can work together and maintain stability in a coupled

DC network without sharing details of their internal designs, across stages of planning, procurement, and operation [5]. To the author's best knowledge, a comprehensive framework and underpinning methodologies to achieve this is missing in the literature.

By introducing constant power terminals driven by the dynamics of offshore wind or system operator's dispatch, a MT-HVDC system is a non-linear system. Aligning with the theory of linearized stability [6], the stability assessment of a non-linear system includes two successive steps, namely the existence of equilibrium and the sufficiency of damping. Although there have been lots of works about the stability of a DC system in both aspects, to the authors' best knowledge, there has not been a comprehensive solution that can ensure both aspects without detailing the internal control of the participating converters. Hence, there is a gap in supporting industrial application of MVMT-HVDC.

In a multi-terminal DC network, a common principle is that at least one terminal must be under the closed-loop voltage regulation [7]. This is to ensure robustness against distributed measurements with respect of power balancing, insulation, and operability of converter. To improve the resilience of an MT-HVDC against loss of the slack DC terminal, control strategies of multiple voltage droops have been proposed to preserve voltage control in 'N-1' conditions and to ensure measurements of DC voltage will not lead to excessive current deviations carried by transfer branches [8]. Such an approach has a benefit in resilience provided the control priorities of such an approach can be defined effectively by the TSOs in a manner that respects the characteristics of the converter response to the objective. To date, the black-boxed nature of these components and lack of clarity in the control architecture required have limited the ability to achieve this. For example, the interactions of droop coefficients will not only impact the operating point but also the small-signal behaviour for which an acceptable control margin must be maintained. The range of voltage variation within the DC system and operating range may be coordinated and regulated by the multi-vendor control to a range of priorities for a range of operating points. A fair criterion to both assess and define the adequacy in the fore cited context is absent, and needs to be presented from a TSO perspective of compatible operation with the interfacing onshore alternating current (AC) transmission system.

As a comparison to three-phase AC system, numerous indexing mechanisms have been proposed for the AC system to quantify the contribution of network to grid strength at the frequency which equilibriums reside on [9, 10] so the small-signal design/analysis can be performed based on it, but this step is missing for HVDC systems.

As for one step towards assessing control interactions in a MVMT-HVDC system, a simple method is proposed here to quantify the domain of operating point, which will serve as a reference at planning and operating stage for follow-up small-signal design and assessment [11]. Without the information of internal design of converters, this method seeks to define the effect of converter response to a variation in terminal voltage such that conditions of stable operation may be identified and directed accordingly. This requires representation of the encrypted control detail within a model/replica in the form of an equivalent control droop response to the voltage change, for a given operating condition. Within that data provision, this method can quantify the interactions of converter controls considering the impact of operating point and the interaction with network metrics.

The rest of the paper is organized as follows. The layout, control architecture, and associate component models of a typical offshore MT-HVDC are introduced in Section 2. It is followed by the principle of the proposed assessment in Section 3. After that, the effectiveness of the proposed methodology is verified in Section 4 by time-domain simulations with a pseudo-steady-state model and a detailed electro-magnetic transient (EMT) multi-modular converter (MMC)–Voltage Source Converter (VSC) model, using *Matlab/Simulink* and real-time digital simulator (RTDS), respectively. Finally, the conclusion is drawn in Section 5.

The contributions of the paper are as follows:

- A framework of control architecture to rigorously plan an HVDC grid without detailing internal design of converter. It allows the converter supplied by vendors to be specified as controllable 'black-boxes', whereas the central control functions as 'white-boxes' defined for system operators.
- Based on the proposed framework, methodologies to quantify the domain of global operating point with a normalized index, which counts in converter design and secondary control design along with the interconnecting electrical network.

2 | METHODOLOGY

2.1 | Benchmark system and analytical model

An illustrative multi-terminal HVDC network interconnecting offshore windfarms and an onshore AC transmission network is considered here. The generic layout of the system is as shown in Figure 1.

As shown in Figure 1, the network consists of two types of HVDC terminal, namely an offshore interfacing wind farm terminal and onshore (OS) terminal. In principle, the more converters participating in the voltage control of the DC network, the greater the flexibility of this control will be; at least one terminal must provide this capability for the overall DC network to be controlled. However, the control of the DC network is subject to practical restrictions in respecting onshore and offshore AC system requirements.

2.2 | Architecture of system control

Based on the scenarios in Section 2.1, a generic control architecture is assumed as shown in Figure 2a. As shown, each converter is covered by a 'black-box' with agreed set of inputs and outputs. Among them, the characteristics of lower-level design are

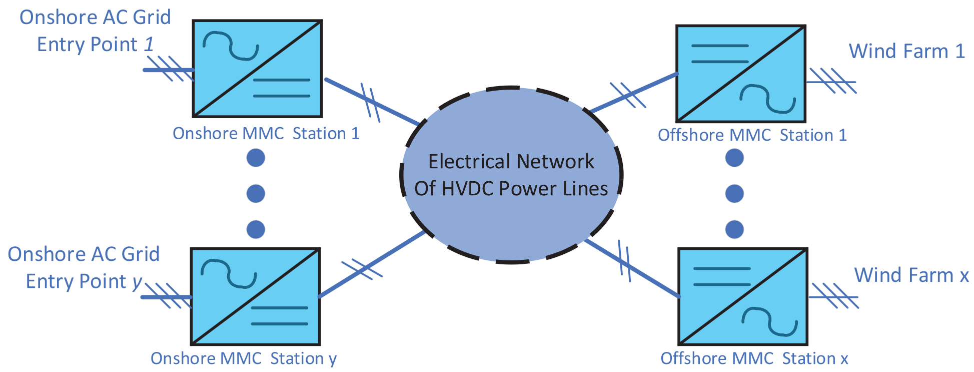

FIGURE 1 Generic layout of an offshore MVMT-high voltage direct current grid.

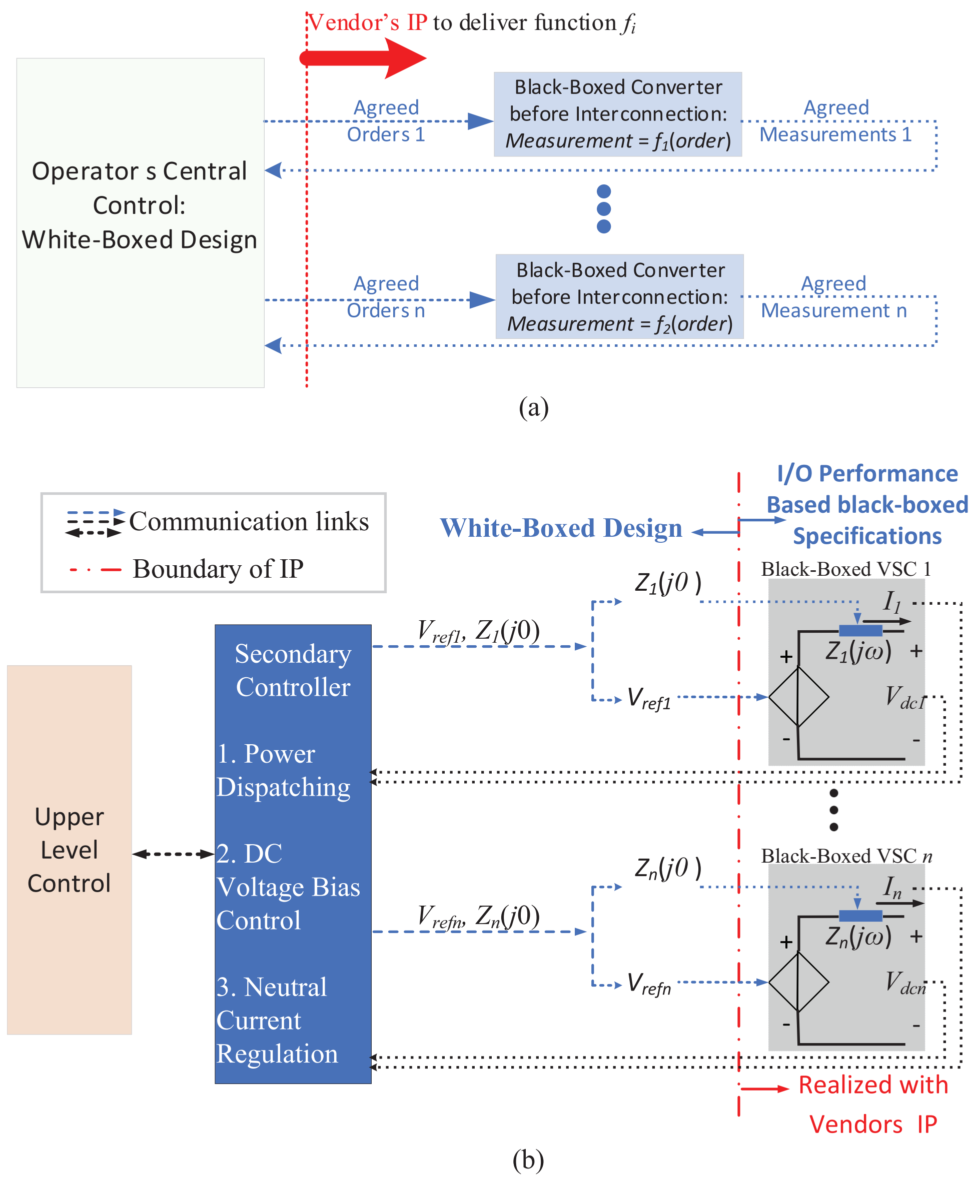

FIGURE 2 Control architecture of MVMT-high voltage direct current grid. (a) Vendor agnostic architecture. (b) Realization of specifications.

aggregated and masked for the protection of vendors' intellectual property (IP). The masked designs include (voltage) regulators of current loops, AC voltage controls, modulation scheme, voltage balancing among sub-modules/arms/phases, main circuit, and other controls related to topology and converter operating principles with respect to both the AC and DC systems. The control performance of ith converter is determined by a time-domain function f_i, such that

$$\overrightarrow{measurement} = f_i\left(\overrightarrow{order}\right) \tag{1}$$

On behalf of TSOs, we propose f_i to be a time-invariant function at steady state, that is, the system is not subject to a step change of structure. Thus, the dynamics of measurements, the output, at its electrical terminal can be linearized when the input orders are fixed around an operating point, which are measurable by TSOs. Thus, at steady state, when the central control and impedances of the electrical network are unchanged, (1) can be rewritten in Laplace domain as

$$F_i\left[\overrightarrow{order\ (s)}\right] = \overrightarrow{measurement\ (s)}, \tag{2}$$

where F_i is the transfer matrix of the converter i after applying Laplace transformation to f_i.

Therefore, the dynamics between the measurement components for each converter is implicitly defined by (1) in time domain and (2) in Laplace (s) domain as a function of input orders and operating point of output measurements.

With a single black-boxed converter model, when the $\overrightarrow{order}$ and $\overrightarrow{measurement}$ are settled across the spectrum, the ratio between a superposed perturbation over the measured quantities and the resultant change of measurement $\Delta\overrightarrow{measurement}(j\omega)$ across frequencies in the spectrum can determine the delivered transfer function between the measured quantities implied by (2) [12]. For application to an HVDC grid, the quantities refer to the voltage and current at DC terminal, which are visible to its TSO and are the interface quantities introducing electrical coupling with the rest of the HVDC grid. In other words, the dynamics between this pair of voltage and current determine the participation of the converter in the interaction with the rest of HVDC grid.

Naturally, the corresponding time-domain dynamics between the voltage and current, implied by (1), can also be inferred from the frequency-domain measurement due to the convertibility among transfer function, frequency-domain response, and time-domain response [12].

2.3 | Realization of control architecture

Realizing the control architecture in an MVMT-HVDC grid, the proposed architecture is as shown in Figure 2b. Corresponding to the principle in Figure 2a, the design in Figure 2b divides the realization into distributed converters covered by 'black-boxes' and operator's centralized control in white-boxes.

2.3.1 | Specifying performance of converter

To avoid excessive liability and advocate vendor agnostic design, we propose TSOs to realize the architecture in Figure 2a by specifying the terminal performance, that is, input/measurement controllability and dynamics between terminal measurements.

The realization of the framework is shown in Figure 2b, where each black-boxed converter, represented by 'VSC i' ($i = 1, 2, \ldots n$) are required to behave as 'a controllable voltage source behind a synthesis impedance'.

The change of the ith controllable source, $V_{\mathrm{ref}i}$, is determined by the secondary control; and the synthesis impedance, Z_i(s), reflect the steady-state DC dynamics of the ith converter on its own. We propose TSOs to keep its 0-rad response dispatchable by secondary control, which is defined as a synthesis resistance R_i (or conductance K_i) such that

$$R_i = Z_i\,(j0) = \frac{1}{K_i} = \frac{V_{\mathrm{ref}i}\,(j0) - V_i\,(j0)}{I_i\,(j0)} \tag{3}$$

The response of the impedance over other frequencies, $Z_i(j\omega)|_{\omega\neq 0}$, will be requested to stay within a domain of three dimensions (which are conductance, susceptance, and frequencies) to cover broad frequencies. The boundaries of the 3D domain are proposed to be specified by TSOs.

As is implied above, we propose TSOs to require full control over the dynamics at 0 rad/s in real-time operation, whereas the dynamics over other frequencies in the spectrum shall be preemptively planned in an off-line manner, that is, keep staying within a fore cited 3D domain specified by TSOs.

As a first step towards HVDC interoperability, the focus of this paper is placed on the response at 0 rad/s, which the equilibrium of a DC system resides on to deliver power; whereas the methodologies of specifying the 3D domain are not in the scope but further detailed in a separate paper [11].

For the offshore AC system providing offshore the wind farm interface, it is normally necessary for grid forming control to be established where the HVDC converter defines the frequency and the voltage of the offshore island [13], thereby representing to the DC system a fixed power flow independent of DC dynamics in its steady-state operation. This needs to be accounted for in the overall solution of the DC network but does not provide further flexibility in defining that solution but rather operates as a consequence of the DC voltage as defined elsewhere within this system, within the range of the DC voltage available. Onshore, the connection interfaces may be operated to a specific intended power flow which does not preclude being set based on a droop power control of the voltage within the DC network, but equally would be dependent also on the operating state of the onshore AC system at the time. Direct control of the AC system, for example at the point of offtake, can be introduced but in the example above would then limit the MVMT network to one point of voltage control and an associated vulnerability to its loss.

Therefore, as to those DC terminals which are entirely driven by local control, for example, actively accommodate the power balancing of the connecting AC network, the form of controllable interfaces in Figure 2b does not affect the terminal measurements; in other words, the dynamics of electrical coupling are independent of the input order.

2.3.2 | Design of central control

As to the central controller, measurements taken from converter terminals are used as feedback to deliver three decoupled functions using closed-loop designs, namely power dispatching, neutral current control, and DC voltage bias control. Based on the feedback measurements, the outputs of the supervisory control will update the incremental values of the agreed order inputs to each black-boxed converter. The proposed autonomous secondary control are as follows:

(i) Power control enables accurate dispatching with a converter without steady-state error.
(ii) Neutral current control eliminates the steady-state neutral current when it flows into earth.
(iii) DC voltage bias control suppresses the common offset of all DC terminals within one pole.

Here, the function of power dispatch is quantified as an illustration to showcase the impact of central control on the quantification of global assessment. The quantification of neutral current control and DC voltage bias control is not in the scope for simplification, but discussed in a separate paper [14] and future work, respectively.

It is also expected that upper-level central control should impose multi-variable optimization to maximize the utilization of transmission infrastructure with power flow-based approach in the realization of Figure 2b, but again its objective and realization are out of the scope of this paper.

Remark. The functions of central controller, including secondary-level and upper-level control, are implemented by a central control unit, which would be owned by the TSOs. As the name implies, the intention of the supervisory control is to course correct the operation of the overall system towards a steady-state condition that is both stable and contingency robust. In this manner, the concept is not dependent on the reliability of communication links as operation for a given condition would remain stable for that operating condition and a range of credible situations ahead of any further update. Actions via the central control would act to slowly modify input orders by the associated converter terminals to correct and drive more secure new operating conditions for the DC network, and transitions of operating state can be implemented via a forward guidance of slow changes over an extended period of time, for example, achieving a ramping up or down of power flow.

2.4 | Nodal model of DC network

Nodal analysis can be applied to quantify the aggregated performance of an HVDC grid, where the equivalent effect of

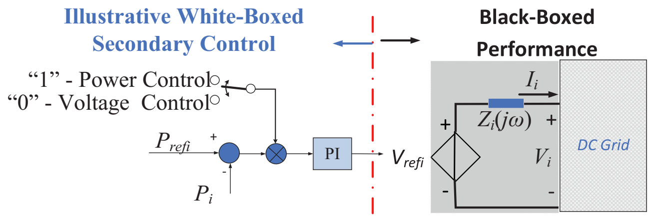

FIGURE 3 Equivalent shunt branch of an MVMT-high voltage direct current grid.

converter, including the applied secondary control, is deemed as impedance of the corresponding shunt branch to TSOs.

Each transfer branch between DC terminals characterizes the aggregated impedance of a corresponding point-to-point DC cable between two nodes and the connected series elements, such as DC circuit breaker, DC reactor, and so on if applicable.

As shown in Figure 3, during operation, the DC terminals with a converter are categorized into two types depending on the enabler in the secondary control, namely voltage dependent, that is, '0'—voltage control, and voltage independent, that is, '1'—power control enabled.

As to a special DC terminal which is not equipped with converter, for example, DC switching station or converter blocked, the admittance of the shunt branch is zero.

Thus, the 0-Hz conductance of a shunt branch is K_i when a converter in voltage control mode is connected; 0 when no converter is connected, and driven by the operating power when a constant power control is enabled in secondary control.

2.5 | Branch model of DC network

For each DC branch, including both the positive and negative poles to give a return path, between nodes i and j, the aggregated impedance, $Z_{ij}(s)$, at steady state is written as

$$Z_{ij}\,(s)\,|_{s=0} = R_{ij} \tag{4}$$

where $R_{ij}(i \neq j)$ is the aggregated resistance of the branch, including return; R_{ii} is the shunt resistance at the ith node.

3 | ASSESSING EXISTENCE OF EQUILIBRIUM

3.1 | Network model at steady state

By interconnecting n nodal equivalents shown in Figure 3 with a branch return in between any two nodes, the equilibriums of an n-node HVDC network can be characterized with Kirchhoff's law [15] for voltage as

$$\boldsymbol{G}\vec{V} = \vec{I} \tag{5}$$

where $\boldsymbol{G}$ is an $n \times n$ diagonal matrix of network conductance; $\vec{V}$ the n-dimension vector of nodal voltage; $\vec{I}$ the n-dimension vector of nodal current injection from converters. Representing the element of $\boldsymbol{G}$ at ith $(0 < i \leq n)$ row and jth $(0 < j \leq n)$ column with G_{ij} gives

$$\begin{cases} G_{ji} = G_{ij} = -\dfrac{1}{R_{ij}} \\ G_{ii} = \displaystyle\sum_{i=1}^{n} \dfrac{1}{R_{ij}} \end{cases} \tag{6}$$

The ith component of $\overrightarrow{V}$ is V_i and ith component of $\overrightarrow{I}$ is I_i. Considering the control in Figures 2 and 3, and assuming the steady-state power at every terminal completely follows the orders dispatched, or the equivalent to accommodate the need of connected AC network, the vector of the nodal current injection can also be expressed as

$$\overrightarrow{I} = \boldsymbol{K}\left(\overrightarrow{V_{\mathrm{ref}}} - \overrightarrow{V}\right) + \boldsymbol{INV}\overrightarrow{P_{\mathrm{ref}}} \tag{7}$$

where $\boldsymbol{K}$ is an $n \times n$ diagonal matrix, whose diagonal element at ith row k_i $(0 < i \leq n)$ represents the voltage droop coefficient of the ith node; if the node is not droop controlled, then $K_{ii} = 0$. $\overrightarrow{V_{\mathrm{ref}}}$ is an n-dimension vector of the reference value of droop control, whose ith $(0 < i \leq n)$ component is $V_{\mathrm{ref}i}$; $\boldsymbol{INV}$ is an $n \times n$ diagonal matrix, whose diagonal element $\boldsymbol{INV_i}$ $(0 < i \leq n)$ is $\frac{1}{V_i}$; $\overrightarrow{P_{\mathrm{ref}}}$ is an n-dimension vector of the arbitrary power injection at all the nodes, whose ith $(0 < i \leq n)$ component $P_{\mathrm{ref}i}$ represents the expected power injection at the ith node.

Substituting (7) into (5), one can define a function

$$\boldsymbol{F}\left(\overrightarrow{V}, \overrightarrow{P_{\mathrm{ref}}}\right) = (\boldsymbol{G} + \boldsymbol{K})\overrightarrow{V} - \boldsymbol{K}\overrightarrow{V_{\mathrm{ref}}} - \boldsymbol{INV}\overrightarrow{P_{\mathrm{ref}}} = 0 \tag{8}$$

Therefore, the vector of terminal voltage is implicitly defined by the function of $\boldsymbol{F}(\overrightarrow{V}, \overrightarrow{P_{\mathrm{ref}}})$ as $\overrightarrow{V} = f(\overrightarrow{P_{\mathrm{ref}}})$.

3.2 | Assessing existence of equilibrium

For the practical design of HVDC networks, the function of $\boldsymbol{F}(\overrightarrow{V}, \overrightarrow{P_{\mathrm{ref}}})$ is a linear combination of polynomial functions and reciprocal functions; hence it is continuously differentiable [16] with respect to all elements of $\overrightarrow{V}$ and $\overrightarrow{P_{\mathrm{ref}}}$. By applying the theorem of implicit function [17] to (8), there must be a unique function of $f(\overrightarrow{P_{\mathrm{ref}}})$ in the neighbourhood of an equilibrium $(\overrightarrow{V_0}, \overrightarrow{P_{\mathrm{ref0}}})$, as long as the following condition stands:

The Jacobi matrix (J) of $\boldsymbol{F}(\overrightarrow{V}, \overrightarrow{P_{\mathrm{ref}}})$ with respect of $\overrightarrow{V}$ is not singular at the equilibrium. That is,

$$|J| = \left|\frac{\partial \boldsymbol{F}\left(\overrightarrow{V}, \overrightarrow{P_{\mathrm{ref}}}\right)}{\partial V_1, \partial V_2, \ldots, \partial V_n}\right|\Bigg|_{\overrightarrow{V} = \overrightarrow{V_0}, \overrightarrow{P_{\mathrm{ref}}} = \overrightarrow{P_{\mathrm{ref0}}}} \neq 0 \tag{9}$$

Starting from an initial equilibrium, the operating point of the HVDC system can be expanded throughout the manifolds that consistently complies with (8) and (9) according to the principle of analytic continuation [16]. It also indicates that the power flow is transferrable. Substituting (8) into (9) yields

$$|\boldsymbol{G} + \boldsymbol{K} + \boldsymbol{INVS}| \neq 0 \tag{10}$$

where $\boldsymbol{INVS} = \{INVS_{ij}\}$ is an $n \times n$ diagonal matrix, whose diagonal element on ith row, $INVS_{ii}$ $(0 < i \leq n)$ is $\frac{-P_{\mathrm{ref}i}}{V_{i,0}^2}$. Define the extended conductance matrix $\boldsymbol{G_{\mathrm{ex}}}$ as

$$\boldsymbol{G_{\mathrm{ex}}} = \boldsymbol{G} + \boldsymbol{K} + \boldsymbol{INVS} = \left\{g_{\mathrm{ex},ij}\right\} \tag{11}$$

where $g_{\mathrm{ex},ij}$ is an element of G_{ex} at ith $(0 < i \leq n)$ row and jth $(0 < j \leq n)$ column.

Since all resistances R_{ij} are positive, (6) ensures the diagonal dominance for the network conductance matrix and positiveness of diagonal element (G_{ii}), which is

$$G_{ii} = \sum_{i=1}^{n} \frac{1}{R_{ij}} \geq \sum_{i=1}^{n} \left|\frac{1}{R_{ij}}\right| > 0 \tag{12}$$

Thus, $\boldsymbol{G}$ is positive definite with the diagonal dominance and the positiveness for practical values of all diagonal elements [18], which can be easily tested at the planning stage. Energizing the HVDC grid with all the power-controlled terminals with zero power, that is, $\overrightarrow{P_{\mathrm{ref0}}} = 0$; considering all elements of the diagonal matrix $\boldsymbol{K}$ must be non-negative for practical designs of the voltage control [7], the diagonal dominance and the positiveness of diagonal dominance is thus preserved for the extended conductance matrix $\boldsymbol{G_{\mathrm{ex}}}$. As a result, $\boldsymbol{G_{\mathrm{ex}}}$ must be positive definite when energizing an HVDC grid [19].

Since the determinant of a positive definite matrix $\boldsymbol{G_{\mathrm{ex}}}$ must be positive and to preserve the existence of equilibrium consistently, (10) is narrowed down to the following condition as

$$|\boldsymbol{G_{\mathrm{ex}}}| = |\boldsymbol{G} + \boldsymbol{K} + \boldsymbol{INVS}| > 0, \tag{13}$$

which indicates the scalar margin of an HVDC grid against the condition of loss-of-equilibrium, that is, $|\boldsymbol{G_{\mathrm{ex}}}| = 0$. Here, $|\boldsymbol{G_{\mathrm{ex}}}|$ is proposed to be the index to define the domain of operating point and indicate the position of operating point.

3.3 | Sensitivity of assessment index

To indicate the operating point in a multi-dimensional domain, the proposed index must preserve a monotonic relationship with the interested dimensions of equilibrium within the domain of operating point. To prove this, a sensitivity analysis of the index $|\boldsymbol{G_{\mathrm{ex}}}|$ is carried out here.

Lemma 1. *From the initialization of the HVDC grid, the continuous domain of operating point that enable* $\boldsymbol{G_{\mathrm{ex}}}$ *preserving the positive* *determinant completely overlap with the positive definiteness as*

$$\{\boldsymbol{G}_{\mathbf{ex}} > 0\} = \{|\boldsymbol{G}_{\mathbf{ex}}| > 0\} \tag{14}$$

Proof by contradiction:

Counter Hypothesis 1: If (14) did not stand for Lemma 1, it can be inferred from (16) that there must have been one set of operating points aligned with the boundary of $\{\boldsymbol{G}_{\mathbf{ex}} > 0\}$ but enclosed by $\{|\boldsymbol{G}_{\mathbf{ex}}| > 0\}$.

Referring to Sylvester's criterion for a real symmetric matrix [18], the determinants of all the leading principal minors ($|M_i|$), that is, the determinant of ith upper left corner matrices of $\boldsymbol{G}_{\mathbf{ex}}$, which includes $\boldsymbol{G}_{\mathbf{ex}}$ itself, are positive as

$$|M_i| > 0 \quad (i = 1, 2, \ldots, n) \tag{15}$$

Thus, one can write

$$\{\boldsymbol{G}_{\mathbf{ex}} > 0\} \subseteq \{|\boldsymbol{G}_{\mathbf{ex}}| > 0\} \tag{16}$$

Referring to the property of a positive definiteness of a real symmetric matrix [18], if and only if within the domain of $\{\boldsymbol{G}_{\mathbf{ex}} > 0\}$, that every eigenvalue of $\boldsymbol{G}_{\mathbf{ex}}$ is positive as

$$\lambda_{\mathrm{ex}i} > 0 \quad (i = 1, 2, \ldots, n) \tag{17}$$

and to breach the sufficient and necessary condition of the positive definiteness of $\boldsymbol{G}_{\mathbf{ex}} > 0$, there must be at least one boundary operating point that breaches (17) as

$$\lambda_{\mathrm{ex}i} = 0 \quad (i = 1, 2, \ldots, \text{ or } n) \tag{18}$$

As the product of all eigenvalues of a matrix always equals to its determinant [20], this property can be applied to $\boldsymbol{G}_{\mathbf{ex}}$ as

$$\prod_{i=1}^{n} \lambda_{\mathrm{ex}i} = |\boldsymbol{G}_{\mathbf{ex}}| \tag{19}$$

Substituting (18) into (19) yields $|\boldsymbol{G}_{\mathbf{ex}}| = 0$, which is contradictory to (16) and the Counter Hypothesis 1.

This completes the proof of Lemma 1.

Proposition 1. *Within the domain of operating point,* $\{|\boldsymbol{G}_{\mathbf{ex}}| > 0\}$*, when the power direction of a voltage-uncontrolled terminal is unchanged,* $|\boldsymbol{G}_{\mathbf{ex}}|$ *is in the monotonic relationship with every power of any voltage-uncontrolled terminal* P_{refi}*, every droop coefficient (*K_i*), and voltage of every voltage-uncontrolled terminal (*$V_{i,0}$*).*

Proof of Proposition 1:

Referring to the definition of the grid conductance matrix G_{ex}, in (6), (7), and (11), it can be inferred that the ith diagonal element ($g_{\mathrm{ex},ii}$) is

$$g_{\mathrm{ex},ii} = K_i + \sum_{i=1}^{n} \frac{1}{R_{ij}} + \frac{P_{\mathrm{ref}i}}{V_{i0}^2} \tag{20}$$

Differentiating (20) with respect to the variables of interest yields

$$\begin{cases} \dfrac{\partial g_{\mathrm{ex},ii}}{\partial K_i} = 1 \\ \dfrac{\partial g_{\mathrm{ex},ii}}{\partial P_{\mathrm{ref}i}} = \dfrac{1}{V_{i,0}^2} \\ \dfrac{\partial g_{\mathrm{ex},ii}}{\partial V_{i,0}^2} = \dfrac{-2P_{\mathrm{ref}i}}{V_{i,0}^3} \end{cases} \tag{21}$$

Expanding $|\boldsymbol{G}_{\mathbf{ex}}|$ with Leibniz formula [18], one can write

$$|\boldsymbol{G}_{\mathbf{ex}}| = \sum_{j=1}^{n} (-1)^{i+j} g_{\mathrm{ex},ij} \left|M_{\mathrm{ex},ij}\right| \tag{22}$$

thus, by definition of $\boldsymbol{G}_{\mathbf{ex}}$, any minor ($|M_{\mathrm{ex},ij}|$) should be independent of the element $g_{\mathrm{ex},ij}$ as

$$\frac{\partial}{\partial g_{\mathrm{ex},ij}} \left|M_{\mathrm{ex},ij}\right| = 0 \quad (i \neq j) \tag{23}$$

Referring to (22) and (23), the sensitivity of $|\boldsymbol{G}_{\mathbf{ex}}|$ with respect of the ith diagonal element $g_{\mathrm{ex},ii}$ is

$$\frac{\partial}{\partial g_{\mathrm{ex},ii}} |\boldsymbol{G}_{\mathbf{ex}}| = \left|M_{\mathrm{ex},ii}\right| \tag{24}$$

Applying chain rule to (21) and (24), the sensitivities of $|\boldsymbol{G}_{\mathbf{ex}}|$ with respect to K_i, $P_{\mathrm{ref}i}$, and $V_{i,0}$ are

$$\begin{cases} \dfrac{\partial}{\partial K_i} |\boldsymbol{G}_{\mathbf{ex}}| = \dfrac{\partial g_{\mathrm{ex},ii}}{\partial K_i} \dfrac{\partial}{\partial g_{\mathrm{ex},ii}} |\boldsymbol{G}_{\mathbf{ex}}| = \left|M_{\mathrm{ex},ii}\right| \\ \dfrac{\partial}{\partial P_{\mathrm{ref}i}} |\boldsymbol{G}_{\mathbf{ex}}| = \dfrac{\partial g_{\mathrm{ex},ii}}{\partial P_{\mathrm{ref}i}} \dfrac{\partial}{\partial g_{\mathrm{ex},ii}} |\boldsymbol{G}_{\mathbf{ex}}| = \dfrac{1}{V_{i,0}^2} \left|M_{\mathrm{ex},ii}\right| \\ \dfrac{\partial}{\partial V_{i,0}} |\boldsymbol{G}_{\mathbf{ex}}| = \dfrac{\partial g_{\mathrm{ex},ii}}{\partial V_{i,0}} \dfrac{\partial}{\partial g_{\mathrm{ex},ii}} |\boldsymbol{G}_{\mathbf{ex}}| = \dfrac{-2P_{\mathrm{ref}i}}{V_{i,0}^3} \left|M_{\mathrm{ex},ii}\right| \end{cases} \tag{25}$$

Referring to Lemma 1, $\boldsymbol{G}_{\mathbf{ex}}$ is positive definite as long as the equilibrium stands and therefore all of its principal minors are positive [18] as

$$\boldsymbol{G}_{\mathbf{ex}} > 0 \Rightarrow \left|M_{\mathrm{ex},ii}\right| > 0 \quad (i = 1, 2, \ldots, n) \tag{26}$$

Since the practical values of terminal voltage must be positive, (25) and (26) guarantee that an increase of K_i and $P_{\mathrm{ref}i}$ will always lead to an increase of $|\boldsymbol{G}_{\mathbf{ex}}|$; and an increase of voltage at the voltage-uncontrolled terminal will lead to a decrease of $|\boldsymbol{G}_{\mathbf{ex}}|$ if the terminal is inverting power; or otherwise, a consistent increase.

This completes the proof of Proposition 1.

Proposition 1 justifies the selection of the index $|\boldsymbol{G}_{\mathbf{ex}}|$ to aggregately indicate the positioning of operating point and set points. To leave a margin against over-loading, over-voltage, and under-voltage, this paper further proposes to define the domain of security as

$$\{D_{\min} < |\boldsymbol{G}_{\mathbf{ex}}| < D_{\max}\}, \tag{27}$$

where $D_{\min}$ and $D_{\max}$ correspond to the boundaries of the domain. Referring to Proposition 1, they can be planned by calculating the values of $|\boldsymbol{G}_{\mathbf{ex}}|$ corresponding to the practical limits of K_i, $V_{i,0}$, and $P_{\mathrm{ref}i}$.

Remark 1. The domain of security defined by (27) does not have to comply with the constraints of power flow. The aggregation of eligible equilibriums is a subset of DC power flow solutions on a mathematical manifold, which is enveloped by (27).

Remark 2. During a steady-state operation, it will be desirable for an operator or a pre-defined power flow controller to know, the setpoint of which terminal is more capable of improving the system security once the index is approaching the boundary of danger. This can be done by carrying out online comparisons between the values of sensitivity in (25). For simplicity, it will not be further discussed here.

3.4 | Normalization of assessment index

The real value of $|\boldsymbol{G}_{\mathbf{ex}}|$ may vary significantly with variable structures of HVDC network metrics or implemented control. This makes it difficult to quantify the equilibrium in a generic manner. To standardize the design, it is better to normalize the indicator.

To normalize of the margin $|\boldsymbol{G}_{\mathbf{ex}}|$, an index named as 'CX-Index I' is proposed as below:

CX-Index I:

$$Ind_{\mathrm{CX1}} = \frac{|\boldsymbol{G}_{\mathrm{ex}}|}{|\boldsymbol{G}_{\mathrm{ex0}}|}, \tag{28}$$

where $\boldsymbol{G}_{\mathrm{ex0}} = G + K$. To obtain the index of (28), the inputs are droop coefficients contained by $\boldsymbol{K}$, network metrics $\boldsymbol{G}$, vector of power injections $\overrightarrow{P_{\mathrm{ref}}}$, and measurements of terminal voltage $\overrightarrow{V}$. Among them, the information of internal design of converters are not required for interoperability.

Given $\boldsymbol{G}_{\mathrm{ex}}$ is positive definite at a no-load condition with all terminal voltage at nominal values and will continue to be positive definite before the loading of power terminal become excessive [21], an alternative of the normalized index (CX-Index II) can also be formulated as

CX-Index II:

$$Ind_{\mathrm{CX2}} = \frac{\lambda(G_{\mathrm{ex}})_{\min}}{\lambda(G_{\mathrm{ex0}})_{\min}}, \tag{29}$$

where $\lambda(A)_{\min}$ refers to the lowest eigen value of matrix A.

Either CX-Index I or II can indicate the positioning of operating point against the loss-of-equilibrium. When the value is closer to 1, it indicates a closer operating condition to a risk-free no-load status, whereas a value more towards 0 indicates a higher risk of loss-of-equilibrium (voltage collapse) [21].

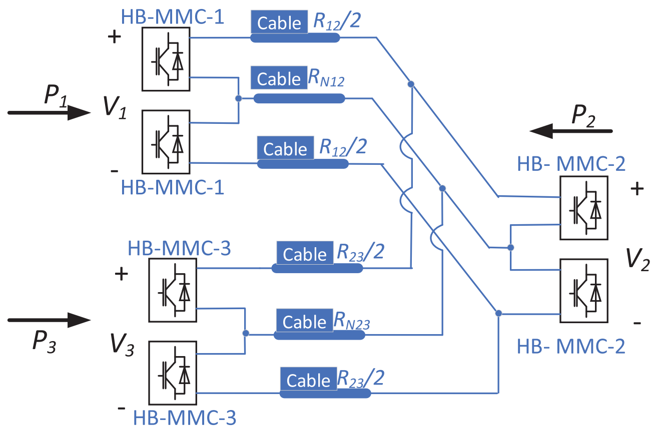

FIGURE 4 Layout of three-terminal benchmark.

3.5 | Inclusion of multi-terminal control

The extended matrix of conductance $\boldsymbol{G}_{\mathbf{ex}}$ can be further expanded by including another component matrix of supervisory droop control (K_s) as

$$\boldsymbol{G}_{\mathbf{ex}} = \boldsymbol{G} + \boldsymbol{K} + \boldsymbol{K}_S - \boldsymbol{INVS}\overrightarrow{P_{\mathrm{ref0}}} \tag{30}$$

where of K_s is an $n \times n$ matrix. Each of its elements K_{Sij} defines the weight of the voltage at jth node ($0 < j \leq n$) towards a global reference value in regulating the voltage at ith node ($0 < i \leq n$). This component can be dispatched by a supervisory control function based on communications between converters and a central control unit. The impact of the communications will be reflected by its non-diagonal elements of K_s. Since such cross-coupling control between terminals does not change the nature of the methodology, $\boldsymbol{K}_S$ is assumed to be a zero matrix for the simplicity in the rest of the paper.

4 | CASE STUDIES

To verify the proposed methodology, a benchmark system is set up for case studies as Figure 4 and Table 1 show.

As shown in Figure 4, a three-terminal bipolar HVDC network is illustrated with all the half-bridge multi-modular converters (HB-MMC) having identical current loops with bandwidth at 600 Hz (referring to an infinite AC bus connection) per pole and control frequency at 20 kHz. Lead–lag regulators are used for all DC regulators with lead and lag time constants at 0.004 and 0.02 s, respectively. Terminal 2 is assigned as a constant power terminal with proportional gain of power regulator at 0.1 kV/MW and time constant at 0.001 s, corresponding to the control scheme in Figure 3.

TABLE 1 Initial parameter of three-terminal benchmark.

Parameter	Value
R_{12}, R_{23}	10 Ω, 10 Ω
Rated voltage	1050 kV (bipolar)
Valve capacitance	43.5 μF (per arm)
K_1, K_3 (equivalent to bipolar)	8.258 A/kV,8.258 A/kV
R_{N12}, R_{N23}	10 Ω, 10 Ω
Timesteps of pseudo-steady-state, EMT simulation	100 μs (Tustin/Backward Euler), 3.57 μs (Dommel)
MMC conduction resistance for EMT simulation (per arm)	0.56 Ω

Two types of models are used for time-domain simulations, namely pseudo-steady-state DC power flow and EMT. The pseudo-steady-state simulation is carried out with *Matlab/Simulink* and the EMT with the real-time digital simulation (RTDS). For pseudo-steady-state simulations, all control and circuits are forced to a steady state, that is, $s = 0$ in the transfer functions; whereas in EMT models, generic average HB-MMC models are used with inter-arm and inter-phase balancing control included [22]. Besides, frequency-dependent models of DC cables [23] are used to simulate DC cables in EMT simulations.

4.1 | Verification of CX-indices in DC power flow

To verify the proposed index, power ramp tests are carried out based on the benchmark system in Figure 4 and Table 1. The results are illustrated in Figure 4.

As shown in Figure 5a, the system starts with the constant power terminal (Terminal 2) operating at 0 MW at time = 0 s. When a power ramp of −1000 MW/s is applied to P_2, the other two terminals start to accommodate this power demand at the same scale as the droop coefficients and network metrics are symmetrical. As the constant power load grows, the voltage at Terminal 2, V_2, decreases from the nominal value of 1050 kV. Meanwhile both CX-Indices (Ind_{CX1} and Ind_{CX2}) drop from the risk-free value of 1, corresponding to the 'no-load energization' condition (all terminals at nominal voltage but operating with no power), towards 0, where the voltage collapse occurs at approximately 4.17 s. Once any of the CX-Indices reaches 0, all quantities start to oscillate chaotically.

As a comparison, the ramp test is repeated with the droop coefficient of Terminal 3 (K_3) reduced by 10% in Figure 5b. This is reflected by a lower power sharing of Terminal 3 in accommodating the constant power demand of Terminal 2.

As a lower droop coefficient leads to a lower grid strength to accommodate the constant power load, the boundary of DC power transfer is reduced to about 3750 MW and collapses at time = 3.75 s, where both CX-Indices again reach zero. This collapse is earlier than in the previous case as expected.

In reality, the voltage saturation limit is more likely to be hit before DC voltage collapse, which implies that the real voltage

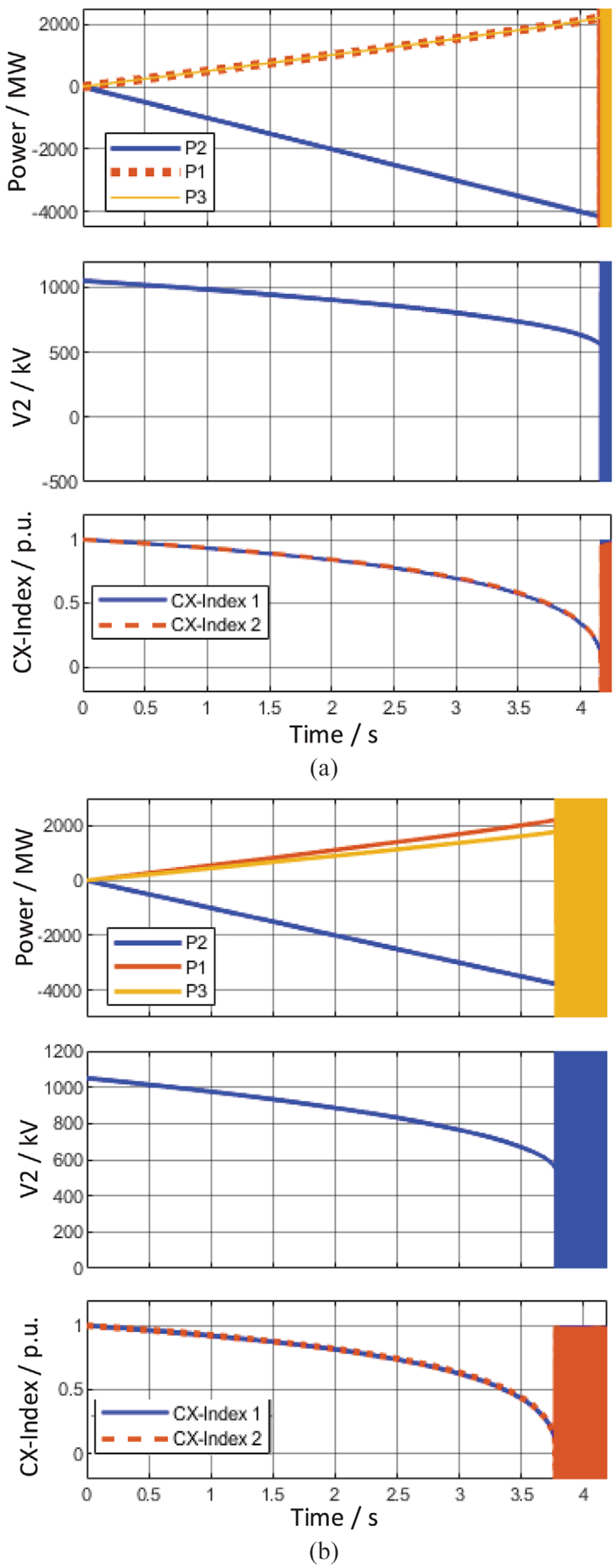

FIGURE 5 Ramp test with pseudo-steady-state simulation: (a) with initial droop coefficients and (b) with reduced droop coefficient.

TABLE 2 Initial parameter of four-terminal-5-node benchmark.

Parameter	Value
$R_{12\pm}, R_{23\pm}, R_{24\pm}, R_{25\pm}$	5.5 Ω
Rated voltage	1050 kV (bipolar)
Valve capacitance	43.5 µF (per arm)
$K_{PH1+}, K_{PH1-}, K_{Eng1+}, K_{Eng1-}$	0.0185 kA/kV
$R_{N12}, R_{N23}, R_{N24}, R_{N25}$	5.5 Ω
Timesteps of pseudo-steady-state, EMT simulation	50 µs (Tustin/Backward Euler), 3.57 µs (Dommel)
MMC conduction resistance for EMT simulation (per arm)	0.56 Ω

is not like to drop the level in Figure 5. The result of this test is mainly to verify the physical meaning of the CX-Indices and its sensitivity against the droop coefficients.

4.2 | Comparison between pseudo-steady-state and EMT simulations

To verify the effectiveness of the CX-Index in an EMT simulation, which is closer to the real-world performance, a comparison is made between simulations with a more realistic EMT model and pseudo-steady-state in Figure 6. Simulation parameters are shown in Table 2.

As shown in Figure 6a, a 4-terminal bipolar MMC EMT average model is established in the environment of RTDS. All terminals, namely PH1, PH2, Eng1, and SP, are interconnected via a switching station as the fifth node. All cables are modelled with a frequency-dependent approach. As shown in Figure 6c, while the HVDC grid is simulated by the RTDS racks, the calculation of CX-Index is performed by a field programmable gate arrays (FPGA)-based external processor, called giga-transceiver system-on-a-chip (GTSOC), with real-time data exchange. The simulation results are captured by the host computer and then presented in Figure 6b.

The setup of the simulation environment is shown Figure 6c. The programmed CX-Index I function in *Matlab/Simulink* is converted to the firmware of GTSOC, which is a FPGA-based processor that can directly convert the function to RTDS compatible function in an encrypted manner. The converted function communicates the pre-defined measurements of power flow and setpoints defined in Section 3.4. to RTDS racks, which simulates the full EMT model in Figure 6a and then feedback the value of CX-Index in every control cycle to RTDS racks. The analytical result of the CX-Index I is then passed to the host computer along with other measurements of interest to generate the results in Figure 6b.

As shown in Figure 6a, PH1 and Eng1 are voltage controlled and PH2 and SP are power controlled in the test. In the results of Figure 6b, SP and PH2 operate at no-load conditions at the beginning of the simulation. From time = 3 s, power ramps of −250 and −125 MW/s are applied to SP and PH2, respectively, until each of them reaches −1000 MW. It can be seen

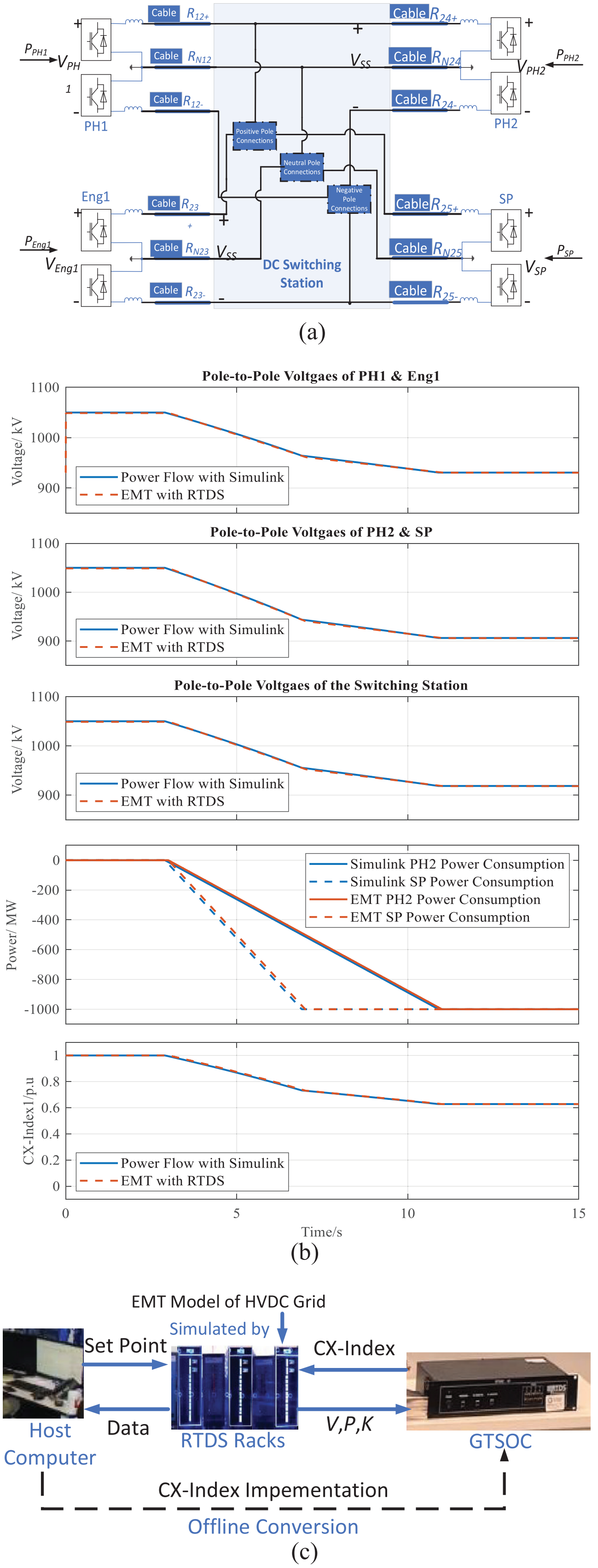

FIGURE 6 Comparison between pseudo-steady-state and electro-magnetic transient: (a) Layout of high voltage direct current grid; (b) Comparison of ramp test; and (c) Simulation platform.

that the EMT measurements of voltage at all terminals drops from the nominal value of 1050 kV down to approximately 860 kV; and CX-Index I drops from 1 to 0.62 simultaneously along with the decreased voltage and the increase of inversion at power-controlled terminals, PH2 and SP. This is aligned with the conclusion in the sensitivity analysis of the index as stated in Section 3.3.

This test is repeated with a pseudo-steady-state simulation with *Matlab/Simulink*. A unit delay of 1.5 s is added to all the powers in the pseudo-steady-state model, which is to make up for the lagging in the power control in the EMT model. It can be seen that the EMT simulation matches well with the pseudo-steady-state simulation with the error lower than 0.3% in the calculating CX-Index throughout the simulation.

Considering the ramp rate and cable resistances are adversely higher than reality, and there are still converter losses that are not taken into account in the DC pseudo-steady-state simulations, the accuracy of the CX-Index I can be regarded as satisfactory.

4.3 | Verification of monotonic sensitivity

To verify the monotonic relationship of the index with respect to terminal voltage, a voltage perturbation is added to both pole ends of the terminal under power control, which is shown in Figure 7a. By fixing the total power of all power-controlled terminals, a ramp of voltage perturbation is added and the corresponding results are captured in Figure 7b.

When the total power injection to the DC grid delivered by power-controlled terminals is −2000 MW, the trajectory of the CX-Index (I) is plotted as the blue curve in Figure 7b, which starts with a value at 0.6282 p.u., corresponding to a resultant bipolar voltage perturbation of 0 kV. By applying a ramp up to 10 kV to the perturbation, the trajectory of the index decreases with the ramp and reaches 0.6239 p.u. when the perturbation is 10 kV. This shows a clear monotonic relationship against voltage increase. This corresponds well to the implication of Proposition 1 in Section 3.3, which implies a monotonic decrease of CX-Index with respect to the voltage of a terminal which is inverting power under power control.

The test of voltage perturbation shown in the blue curve is repeated with a lower total power of inversion, −600 MW, and the trajectory of the index is again plotted in Figure 7b as the brown curve. It shows again a consistent decrease of index with respect to the voltage increase, at a lower magnitude, that is, from 0.901 to 0.9 p.u. This again is aligned with Proposition 1 and the lower magnitude is caused by the lower contribution of power towards the index, which is implied by (21) and (22).

Similar tests are repeated with identical voltage perturbation applied. By setting the total power dispatched by the power terminal as 600 and −600 MW, the corresponding CX-Index (I) are plotted as the blue (1.091 to 1.0918) and brown (0.901 to 0.9) curves in Figure 7c, respectively. Comparing both curves in Figure 7c, when the controlled power is rectification, the sensitivity of the index with respect to terminal voltage is positive,

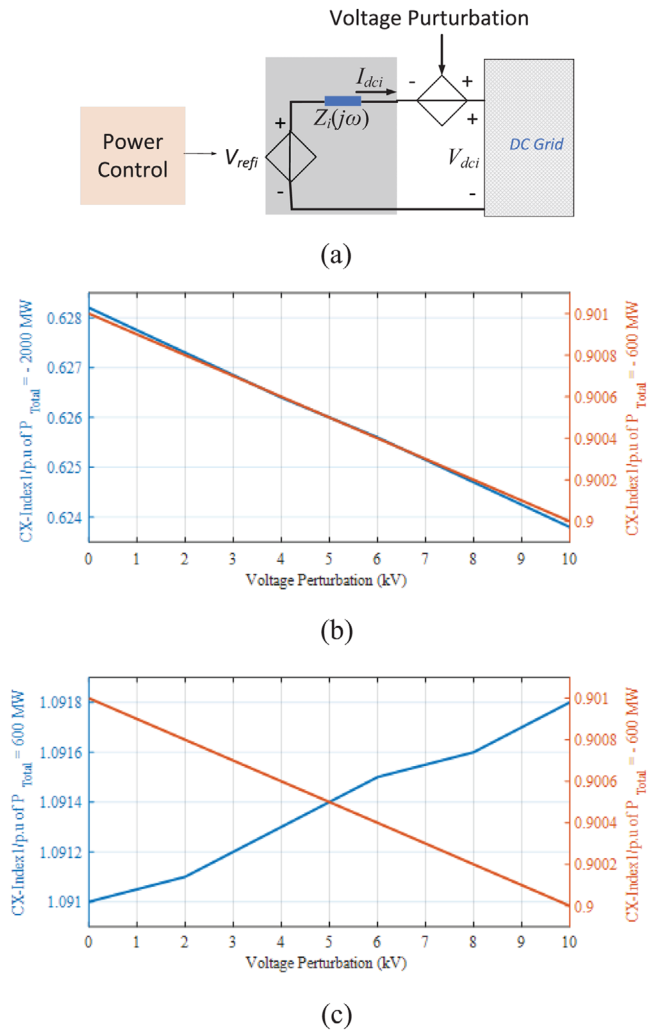

FIGURE 7 Verification of monotonic sensitivity of CX-Index I: (a) Introduction of voltage perturbation; (b) Trajectory with inversion power; and (c) Comparison between inversion and rectification.

whereas the negative power leads to a negative sensitivity with inverse slope.

Comparing both brown curves in Figure 7b,c, it can be seen that a more negative operating power leads to lower CX-Index with the same operating voltage. This corresponds well with the expected index sensitivity against the dispatched power in Proposition 1.

4.4 | Limitations of the simulation tools

With the great recognition and acceptance in both academic and industrial research, *Matlab/Simulink* and RTDS have been used for the initial analysis and validation. However, both tools still have inherent limitations in fully replicating real-world HVDC systems.

For instance, non-linearities in power electronics, which may emerge under specific operating conditions, are simplified in simulations of the adopted Matlab pseudo-steady-state model, leading to discrepancies between modelled and actual system responses. Additionally, environmental factors, that is, temperature variations and mechanical stresses; as well as hardware imperfections, that is., aging effects, tolerances in components, communication interference, or variations in manufacturing are not typically captured in simulation environments yet. Lastly, the variation of real-world cable impedance, fluctuating AC dynamics, and the impedance of earth, is difficult to model with complete accuracy at planning stage, limiting the simulations' ability to fully represent the operational behaviour of such systems. And such limitations in modelling the electrical plant calls for a sufficient margin of grid performance and its sensitivity shall be reflected in the specifications of HVDC converter design.

As to the accuracy of converter control, the collaborations with multiple industrial partners will involve testing vendor-specific converter controls within a black-boxed environment, delivered in the format of software-in-the-loop, for example, GTSOC, and/or control hardware-in-the-loop, for example, real-world control cubicles (replica), addressing the limitations of simulation tools by offering insights into the performance of the system under real-world operational stresses and complexities. This will help reduce the gap between simulation-based validation and actual HVDC system behaviours.

Building on the current work, the analysis presented here is part of an on-going work to quantify an operating domain of small-signal stability, which has been partially and will be published in the future as discussed in Section 2.3.2.

The simulation results presented in Section 4 provide preliminary evidence and a foundation for further analysis involving more complex HVDC systems. Future work will include different realizing approaches from multiple vendors to assess the robustness of the CX-Index under varying conditions to evaluate their impact on the control framework's accuracy.

5 | CONCLUSION

This paper provides a compact mathematical and simulation proof of the concept of a MVMT-HVDC control paradigm not reliant upon the open disclosure, modification, or standardization of the core intellectual property of a converter control. Rather via clear definition and solution of the DC network condition based upon the representation of the effect of the converter control, and a definition of margin in that operation relevant to the steady-state stability, an overall, non-vendor specific solution may be obtained in alignment to the TSOs' priorities for intended operation of the DC network. Therefore, this allows both the MVMT-HVDC control and the associated converter contributions to it, to be described, designed, specified, tested, and deployed with clear definition of individual vendor role and performance.

With reference to the proof, the proposed indices, namely CX-Index, can effectively quantify the interactions among converter droop coefficient, the DC network metrics and operating points within a HVDC network. Either index can generically indicate security margin against DC power transfer limit. With the monotonic relationship with voltages and power of voltage-uncontrolled terminals as well as all droop coefficients, CX-Index thus can be employed to quantify the domain of security and positioning of operating point by comparing the index value with '1'. A closer proximity indicates a better security margin.

Although this indexing methodology is derived from static behaviour of an HVDC system, real-time EMT simulations show that it can provide good accuracy in an online assessment from one steady-state to a new steady-state operation across a transition of a significant power ramp.

AUTHOR CONTRIBUTIONS

Dong Chen: Conceptualization; data curation; funding acquisition; investigation; methodology; project administration; resources; supervision; validation; visualization; writing—original draft; writing—review and editing. **Pimonpan Phurappa**: Formal analysis; investigation; resources; validation; visualization; writing—review and editing. **Benjamin Marshall**: Conceptualization; funding acquisition; methodology; resources; supervision; writing—original draft; writing—review and editing. **Adam Scott**: Formal analysis; investigation; software; validation. **Callum Henderson**: Software; writing—review and editing.

ACKNOWLEDGEMENTS

This paper is an invited expansion version of the following paper published in *IET Conference AC/DC Transmission 2023*: Dong Chen, et al., "Towards HVDC Interoperability—Assessing Existence of Equilibrium with Reference to Converter Terminal Behaviour" [21]. The authors would like to thank the support from Dr. Michael Merlin with University of Edinburgh, Prof. Mohammad Abusara with University of Exeter, and Dr. Haibing Wang with University of Strathclyde. The project is funded by the projects of "Aquila Interoperability Packaged" and "Aquila Lite" with SSEN Transmission and partially funded by the project of "HVDC Control" with the EPSRC Industrial Doctoral Centre for Offshore Renewable Energy (IDCORE).

CONFLICT OF INTEREST STATEMENT

The authors declare no conflicts of interest. The publication was processed by independent editors.

DATA AVAILABILITY STATEMENT

The data that support the findings of this study are available from the corresponding author upon reasonable request.

ORCID

Dong Chen https://orcid.org/0000-0001-8161-2794
Pimonpan Phurappa https://orcid.org/0009-0006-8567-4726

REFERENCES

1. HM Government Department for Business, Energy & Industrial Strategy: Net zero strategy: Build back greener. https://www.gov.uk/government/publications/net-zero-strategy. Accessed 07 Nov 2022

2. National Grid ESO: The pathway to 2030 holisitic network design. https://www.nationalgrideso.com/future-energy/the-pathway-2030-holistic-network-design. Accessed 07 Nov 2022
3. Lu, W., Ooi, B.-T.: Premium quality power park based on multi-terminal HVDC. IEEE Trans. Power Delivery 20(2), 978–983 (2005)
4. The National HVDC Centre: Caithness-Moray HVDC project during delivery. https://www.hvdccentre.com/our-projects/caithness-moray/. Accessed 07 Nov 2022
5. Shetgaonkar, A., Liu, L., Lekić, A., Popov, M., Palensky, P.: Model predictive control and protection of MMC-based MTDC power systems. Int. J. Electr. Power Energy Systems 146, 108710 (2023)
6. Saat, M.S.M., Nguang, S.K., Nasiri, A.: Analysis and Synthesis of Polynomial Discrete-Time Systems: An SOS Approach. Butterworth-Heinemann, Oxford (2017)
7. Beerten, J., Van Hertem, D., Belmans, R.: VSC MTDC systems with a distributed DC voltage control-A power flow approach. In: 2011 IEEE Trondheim PowerTech, pp. 1–6. IEEE, New Jersey (2011)
8. Liang, J., Jing, T., Gomis-Bellmunt, O., Ekanayake, J., Jenkins, N.: Operation and control of multiterminal HVDC transmission for offshore wind farms. IEEE Trans. Power Delivery 26(4), 2596–2604 (2011)
9. Henderson, C., Egea-Alvarez, A., Kneuppel, T., Yang, G., Xu, L.: Grid strength impedance metric: An alternative to SCR for evaluating system strength in converter dominated systems. IEEE Trans. Power Delivery 39(1), 386–396 (2024)
10. Zhang, F., Xin, H., Wu, D., Wang, Z., Gan, D.: Assessing strength of multi-infeed LCC-HVDC systems using generalized short-circuit ratio. IEEE Trans. Power Syst. 34(1), 467–480 (2019)
11. Chen, D., Marshall, B.: Towards HVDC interoperability—On dominance of nodal impedance (2023). https://doi.org/10.36227/techrxiv.24412258
12. Skogesta, S., Postlethwaite, I.: Chapter 2 - Classical feedback control. In: Multivariable Feedback Control Analysis and Design, pp. 15–20. John Wiley & Sons, Hoboken, NJ (2010)
13. Rathnayake, D.B., et al.: Grid forming inverter modeling, control, and applications. IEEE Access 9, 114781–114807 (2021)
14. Chen, D., Phurappa, P., Marshall, B., Ahmad, M.W., Henderson, C.: Towards HVDC Interoperability-Neutral Current Control for Multiple Terminals. EasiyChair Preprint 13292. May 15, 2024
15. Boylestad, R.L.: Introductory Circuit Analysis. Pearson Education, London (2013)
16. Churchill, R., Brown, J.: Complex Variables and Applications. McGraw Hill, New York (2014)
17. Krantz, S.G., Parks, H.R.: The Implicit Function Theorem: History, Theory, and Applications. Springer Science & Business Media, Berlin (2002)
18. Strang, G.: Introduction to Linear Algebra. Wellesley-Cambridge Press, Wellesley, MA (1993)
19. Duran, A.J.: On orthogonal polynomials with respect to a positive definite matrix of measures. Canad. J. Math. 47(1), 88–112 (1995)
20. Teufl, E., Wagner, S.: Determinant identities for Laplace matrices. Linear Algebra App. 432(1), 441–457 (2010)
21. Chen, D., Marshall, B., Foote, C., Rangasamy, S., Tian, S.: Towards HVDC interoperability—Assessing existence of equilibrium with reference to converter terminal behaviour. In: 19th International Conference on AC and DC Power Transmission (ACDC 2023), pp. 224–231. Glasgow, UK (2023). https://doi.org/10.1049/icp.2023.1333
22. Guo, D., Rahman, M.H., Ased, G.P., Xu, L., Emhemed, A., Burt, G., et al.: Detailed quantitative comparison of half-bridge modular multilevel converter modelling methods. J. Eng. 2019(16), 1292–1298 (2019)
23. Beerten, J., D'Arco, S., Suul, J.A.: Frequency-dependent cable modelling for small-signal stability analysis of VSC-HVDC systems. IET Gener. Transm. Dis. 10(6), 1370–1381 (2016)

How to cite this article: Chen, D., Phurappa, P., Marshall, B., Scott, A., Henderson, C.: Towards HVDC interoperability—Vendor agnostic control architecture and quantifying domain of operating point. IET Gener. Transm. Distrib. 19, e13298 (2025). https://doi.org/10.1049/gtd2.13298